

## Electronic Supplementary Information

### Complex study of the fast blue luminescence of oxidized silicon nanocrystals:

#### The role of the core

Lukáš Ondič,<sup>1,2, a)</sup> Kateřina Kůsová,<sup>1</sup> Marc Ziegler,<sup>2</sup> Ladislav Fekete,<sup>3</sup> Viera Gärtnerová,<sup>3</sup> Vladimír Cháb,<sup>3</sup> Václav Holý,<sup>4</sup> Ondřej Cibulka,<sup>1</sup> Kateřina Herynková,<sup>1</sup> Mathieu Gallart,<sup>2</sup> Pierre Gilliot,<sup>2</sup> Bernd Hönerlage,<sup>2</sup> and Ivan Pelant<sup>1</sup>

<sup>1)</sup>*Institute of Physics, Academy of Sciences of the Czech Republic, v.v.i.,  
Cukrovarnická 10, 162 53, Prague 6, Czech Republic*

<sup>2)</sup>*IPCMS, CNRS and Université de Strasbourg, 23, rue du Loess,  
F-67034 Strasbourg, France*

<sup>3)</sup>*Institute of Physics, Academy of Sciences of the Czech Republic, v.v.i.,  
Na Slovance 1999/2, 182 21, Prague 8, Czech Republic*

<sup>4)</sup>*Faculty of Mathematics and Physics, Charles University, Ke Karlovu 3,  
121 16 Prague 2, Czech Republic*

---

<sup>a)</sup>Electronic mail: [ondic@fzu.cz](mailto:ondic@fzu.cz)

# I. STRUCTURAL AND MICROSCOPY CHARACTERIZATION

In this section, results of the structural characterization of silicon nanocrystals (SiNCs) investigated in this study are presented.

## A. X-ray diffraction measurements

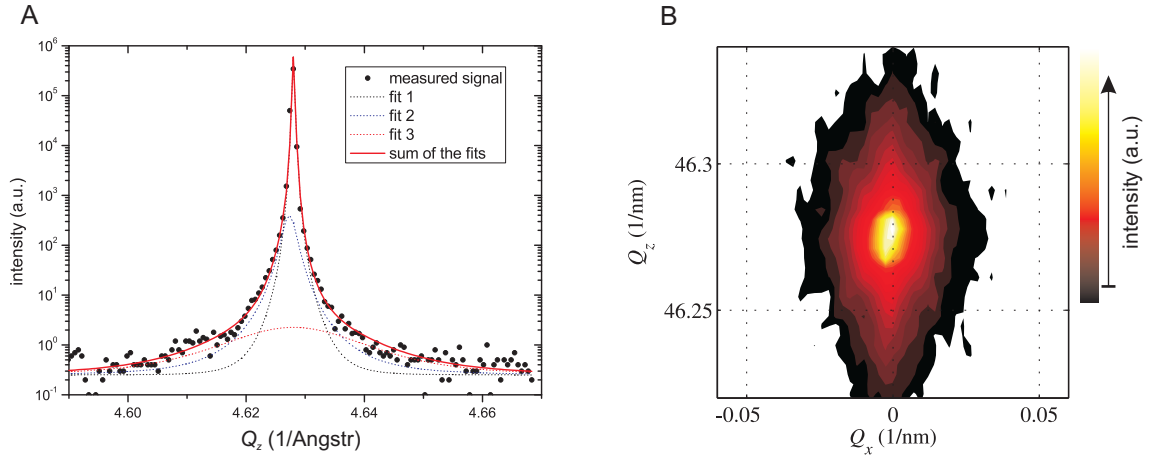


Figure S 1: Results of X-ray diffraction measurements conducted on a porous layer comprising interconnected SiNCs on a Si wafer.: (A) symmetric  $\omega/2$  theta scan, (B) two-dimensional reciprocal space maps. The step of the iso-intensity contours is  $10^{0.25}$ . Both measurements were taken in symmetric geometry around the 004 diffraction maximum.

X-ray diffraction (XRD) measurements were carried out on as-prepared porous layer of SiNCs attached to a Si wafer around the symmetric 004 maximum. Figure S1A plots the  $\omega/2$  theta scan fitted with three functions. The narrower component is the substrate peak and the broadest component originates from the SiNCs. Figure S1B shows a reciprocal-space map. The vertical narrow streaks stems from the substrate, whereas the broader elliptical cloud is due to the nanocrystals. The fact that this cloud is vertically elongated implies that the shape of SiNCs is slightly laterally elongated. However, the influence of inhomogeneous elastic deformation in the nanocrystals is neglected, which broadens the nanocrystals maximum too.

## B. Atomic force microscopy (AFM) measurements

Highly diluted colloidal suspension of SiNCs in ethanol was drop-casted on a Si wafer and investigated by the AFM method. Figure 2 shows the representative image of a line profile taken from the measured AFM image. Figure 3 shows the AFM images taken at four different places on the sample.

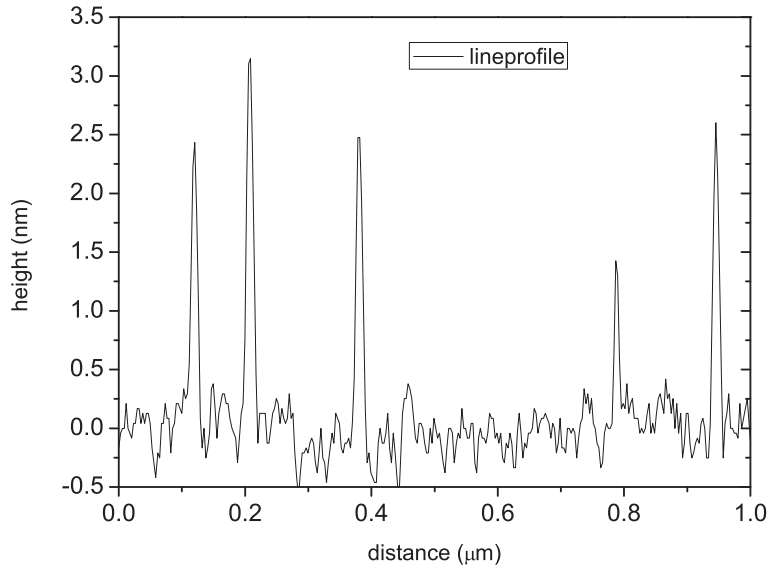


Figure S 2: A line profile taken from an AFM image measured on SiNCs drop-casted on a Si wafer. It manifests that the lateral dimensions of the nanoparticles are broadened due to the convolution with the AFM tip. On the other hand, the measured heights represents correct values.

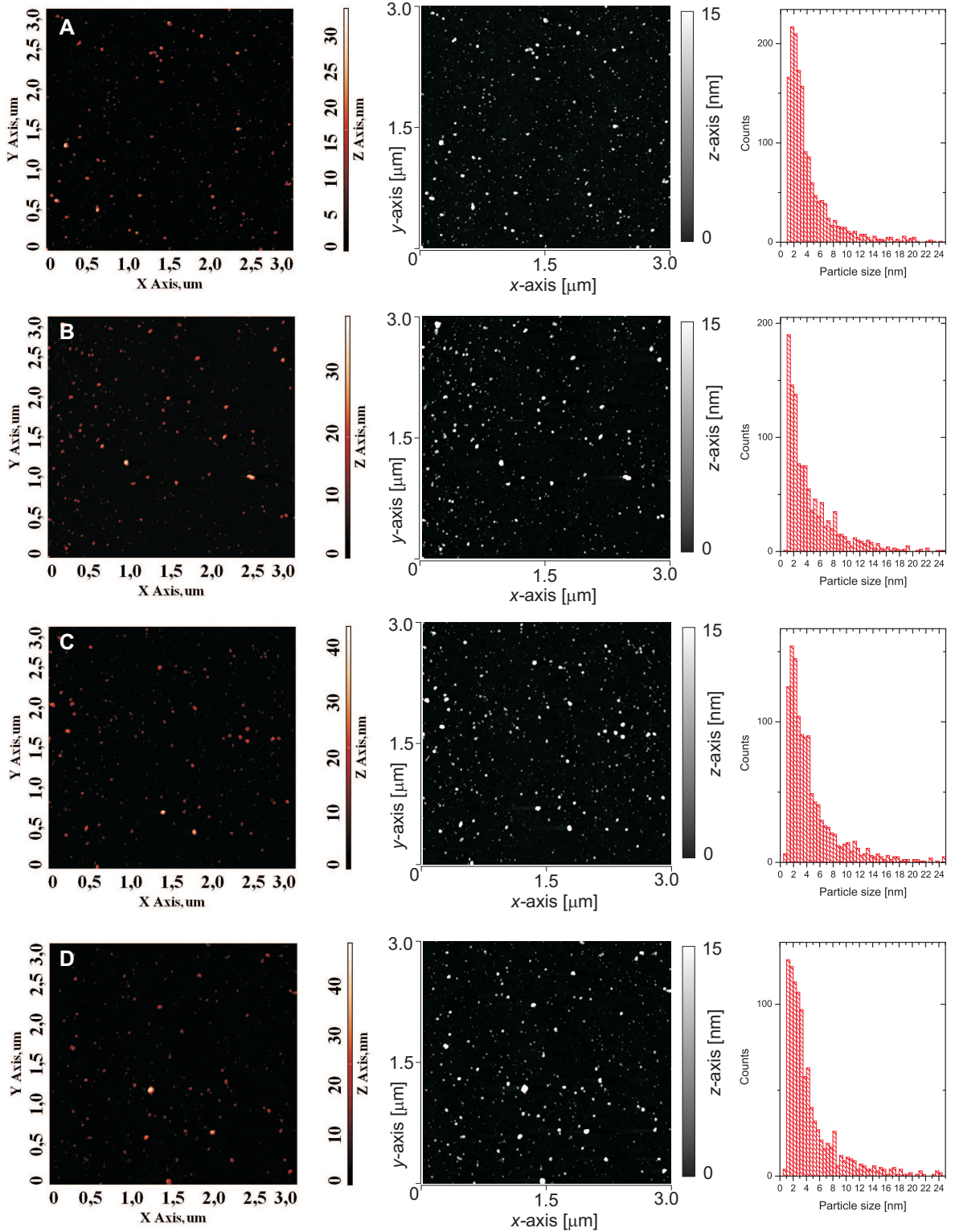


Figure S 3: AFM images from four different places on the sample. Each row comprises: (i) the AFM image with the z-axis normalized to the size of the tallest object, (ii) the AFM image (in blackwhite color scale) with the z-axis normalized to 15 nm in order to enhance the visibility of smaller SiNCs, and (iii) a histogram of the sizes of the objects derived from the images on the left.

## II. OPTICAL CHARACTERIZATION

### A. Measurements in the 2 $\mu\text{s}$ temporal window.

The S-band photoluminescence (PL) spectra of silicon nanocrystals (SiNCs) at 4 K and at room temperature are shown in Figs. S4A and B, respectively. In order to compare the S-band intensity at the beginning and at the end of the 2  $\mu\text{s}$  detection time window, signal was integrated over a 100 ns long time interval at the time delay of 100 ns (black curve) and 1.7  $\mu\text{s}$  (red curve). Even though the signal is noisy, it is evident that the S-band PL intensity drops only negligibly for both temperatures (slightly more for the room temperature). This shows that the S-band does not fully relax between two consecutive excitation events, separated in time by a 5  $\mu\text{s}$  interval.

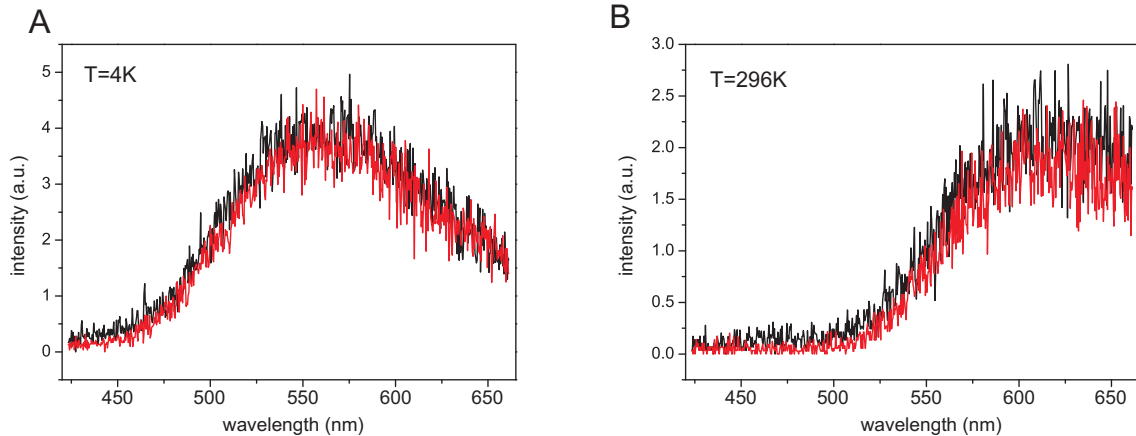


Figure S 4: The S-band emission spectra of SiNCs integrated over a 100 ns time interval, taken at different time delays: 100 ns (black curve) and 1.7  $\mu\text{s}$  (red curve) after the excitation event at 4K (A) and room temperature (B).

### B. Measurements in the 10 ns temporal window.

Normalized PL spectra taken at the beginning (integrated from 0 to 0.5 ns) and at the end (integrated from 8.5 to 9 ns) of the 10 ns time window are shown in Figs.S5 (A1) and (B1) for 4K and room temperature, respectively. Very similar F-band redshift with time was measured for both temperatures. In order to demonstrate that the red-shift of the F-band with time (at least in the first 10 ns after excitation) is not caused by the decrease

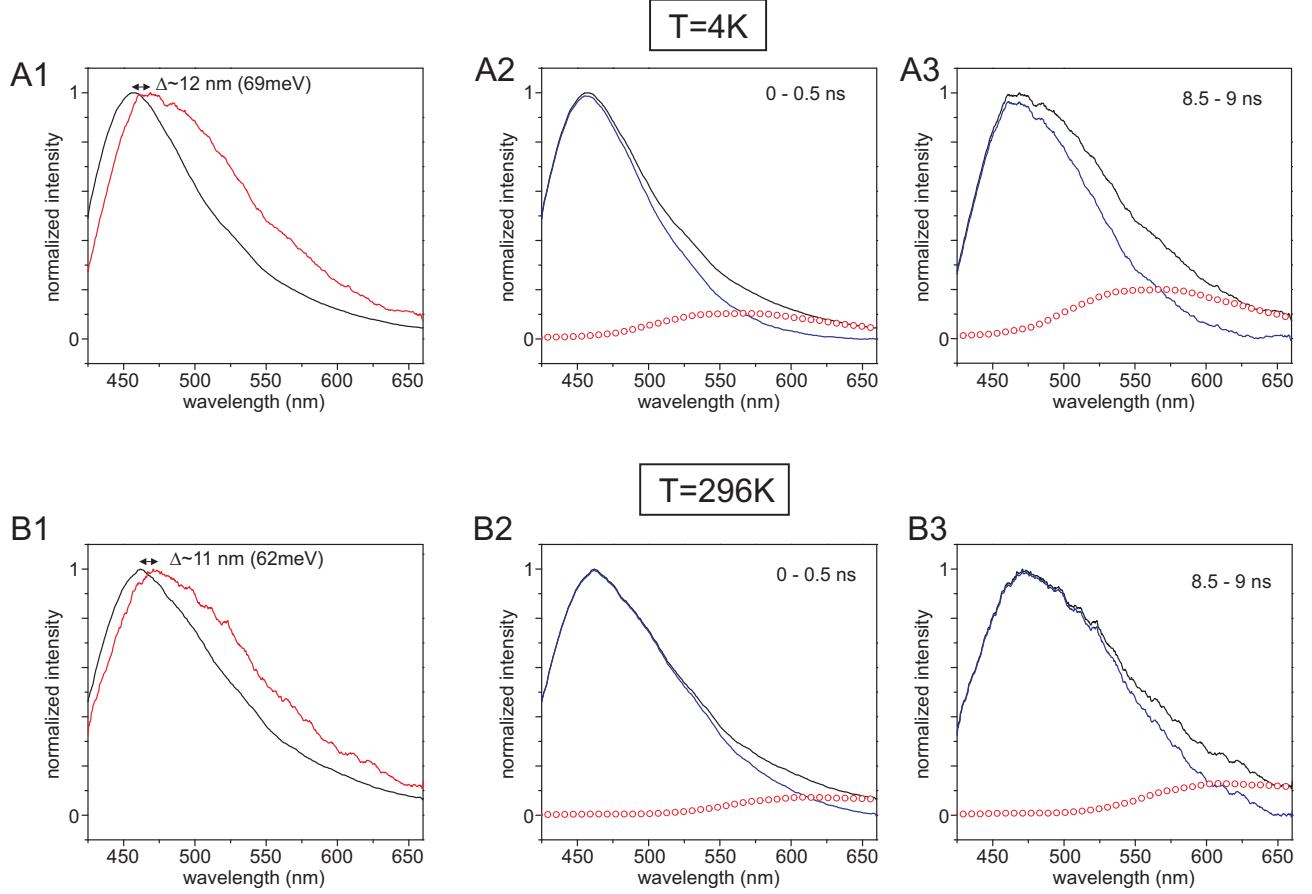


Figure S 5: The F-band’s red-shift with time delay at 4 K (A1) and at 296 K (B1) is demonstrated by plotting the PL spectra integrated over the time window of 0-0.5 ns (black curve) and 8.5-9 ns (red curve). The A-row (B-row) comprises of spectra taken at 4 K (296K). (A2-3) and (B2-3) depict the difference spectra (blue curve) obtained as a difference between the measured F-band spectra (black curve) and the normalized S-band spectra (red opened circles) integrated over the time window  $t = 0 - 0.5\text{ ns}$  (A2, B2) and  $t = 8.5 - 9\text{ ns}$  (A3, B3).

of its intensity compared to the S-band intensity, we plot the difference (blue curve) of the F-band (black curve) and the S-band (red open circles) spectra (Figs.S5 (A2-3), (B2-3)). We assumed that the orange-red part (tail) of the F-band is caused by the S-band admixing and therefore, the S-band spectra were normalized so that their long-wavelength wing matches the F-band’s orange tail. This gives us the upper estimate of the possible S-band’s influence. PL peak positions of the difference spectrum and the measured F-band spectrum agree in the case of spectra taken at  $t = 8.5 - 9\text{ ns}$  at room temperature and at  $t = 0 - 0.5\text{ ns}$  at both K and room temperature, see Figs.S5(A2), (B2) and (B3). There is only a negligible

difference in the case of the spectra at  $t = 8.5 - 9$  ns at 4 K, see Fig.S5(A3). Based on this observation, we can claim that the measured F-band's red-shift with time (at least in the first 10 ns after excitation) is its intrinsic property.

The F-band spectra integrated over the whole detection time window of 10 ns are shown in Fig.S6. The spectra are plotted in a temperature range going from 4 K to 296 K, with the step of 50 K. PL maximum shifts with increasing temperature from about 460 to 466 nm, which is approximately 35 meV. An energetically equal red-shift was also measured in the time window of 2 ns (see the main text).

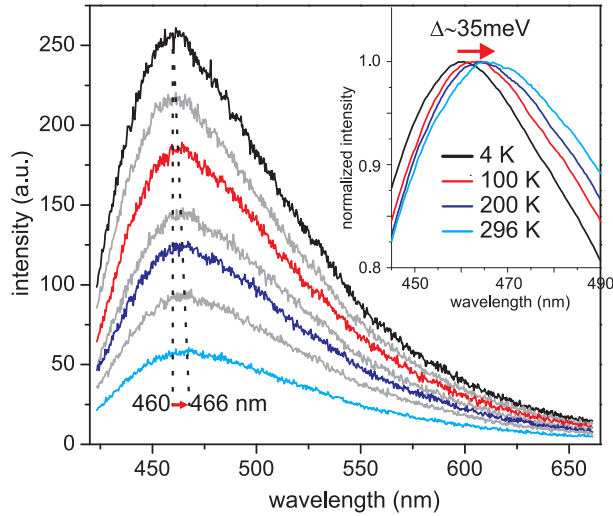


Figure S 6: Temperature dependent PL spectra integrated over a 10 ns detection window. Spectra start at 4K (black curve) and finish at 296K (light blue curve) with the step of about 50 K. The inset depicts normalized PL spectra zoomed-in around the signal maximum for selected sample temperatures.

### III. COMMENT ON THE TEMPERATURE-INDUCED SHIFT OF THE F-BAND SPECTRAL MAXIMUM

The interpretation of the F-band as a quasi-direct recombination between the levels near the  $\Gamma$ -point is also supported by the observed relatively low dependence of the F-band's spectral location on sample temperature. It can be partly explained by considering the effect of tensile strain on the Si direct band gap. It is well-known that the direct band gap of bulk Si becomes wider by about 30 meV upon 296K  $\rightarrow$  4 K cooling<sup>1</sup>. However, the situation is

not so straightforward in free-standing SiNCs with oxide-capping. In bulk Si, cooling of the material decreases the amplitude of Si-atom vibrations around their equilibrium positions, which results in a reduced overlap of electron clouds and thereby it induces shrinking of the conduction and valence band widths, increasing the bandgap value. This is, however, to a certain extent compensated by the increased overlap of the electronic wavefunctions caused by the fact that Si atoms are getting closer to each other upon cooling. In free-standing SiNCs covered with a SiO<sub>2</sub> shell, as used in the present study, on the one hand the cooling-induced contraction of the silicon lattice is substantially reduced because of the much larger thermal expansion coefficient of silicon compared to SiO<sub>2</sub>, i.e. Si atoms in SiNCs are held back by the SiO<sub>2</sub> shell ( $\rightarrow$ tensile strain) and thus almost do not move compared to those in bulk when cooling down. This should lead to a larger temperature variation of the band gap in our SiNCs than in bulk Si.

On the other hand, because of the negative sign of the  $a(\Gamma_{15}) - a(\Gamma'_{25})$  deformation potential<sup>2</sup>, the introduced tensile strain will act against the direct (F-band) band gap opening (Fig. 6 in the main text) and the balance between these two phenomena might explain the observed small value of  $\sim 35$  meV for the temperature-induced shift. Moreover, the positive sign of the deformation potential pertinent to the silicon indirect band gap ( $\Delta_{conduction} - \Gamma_{valence}$ ) makes the tensile strain cooperate with the cooling-induced widening of the indirect band gap (47 meV in bulk Si<sup>2</sup>) and, therefore, enables us to explain in a natural way the observed very large indirect (S-band) gap opening of 200 meV (Fig. 6 in the main text). In order to support this idea quantitatively, however, reliable data on thermal expansion coefficients of 3 nm SiNCs and/or theoretical computations would be needed.

## REFERENCES

- <sup>1</sup>A. Dargys and J. Kundrotas, *Handbook on physical properties of Ge, Si, GaAs and InP*, Science and Encyclopedia Publishers, Vilnius, 1994.
- <sup>2</sup>P. Yu and M. Cardona, *Fundamentals of Semiconductors*, Springer, Berlin, 1996.